Comparative Investigation of Zeolitic imidazolate frameworks(ZIF)-Derived Electrocatalysts for Oxygen and Urea Oxidation Reactions

Benchmarking Ni Foam, ZIF-8, and ZIF-67-Derived Electrodes for Alkaline OER/UOR

Hatem Saleh Al-Mutairi

hatim.almutairi@kaust.edu.sa

Mentor: Guanjie He

August 8, 2026

Abstract

Developing efficient anodic electrocatalysts is essential for reducing the energy consumption of electrochemical hydrogen production, while replacing the sluggish oxygen evolution reaction (OER) with thermodynamically favourable small-molecule oxidation provides a promising route toward more energy-efficient electrolysis. Here, we present a comparative investigation of ZIF-based electrocatalysts for oxygen and urea oxidation reactions (UOR), in which ZIF-8 and ZIF-67 electrodes are systematically benchmarked against Ni foam under alkaline conditions. The electrocatalytic activity, reaction kinetics, and interfacial charge-transfer behaviour were evaluated using cyclic voltammetry, linear sweep voltammetry, Tafel analysis, and electrochemical impedance spectroscopy in 1 M KOH with and without urea. In pure KOH, Ni foam exhibited an overpotential of 316 mV at 10 mA cm^{-2}, compared with 164 mV for ZIF-8 and 369 mV for ZIF-67, although the apparent low-potential response of the ZIF-based electrodes requires careful interpretation because of capacitive and surface-redox contributions. Upon introducing urea, the anodic oxidation potentials decreased substantially, with ZIF-67 requiring only 146 mV at 10 mA cm^{-2}, compared with 205 mV for Ni foam and 224 mV for ZIF-8. Tafel analysis further revealed slopes of 24, 82, and 90 mV dec^{-1} for Ni foam, ZIF-8, and ZIF-67, respectively, under UOR conditions, demonstrating distinctly different reaction kinetics among the electrodes. A supplementary long-term chronopotentiometric hold (100 mA cm^{-2}, ~26 h) further showed that the ZIF-67 electrode reaches a quasi-steady operating potential within ~1–1.5 h and sustains it over the full test duration. Overall, this comparative study highlights the strong influence of the metal centre and electrochemically reconstructed surface on alkaline OER/UOR behaviour and establishes a basis for the rational development of MOF-derived electrocatalysts for energy-saving hydrogen production.

Contents

Abstract **2**

1 Introduction **4**

2 Related Work **4**

3 Methodology **5**

3.1 Materials synthesis 5

3.2 Electrochemical measurements 6

3.3 Data analysis 6

4 Results **6**

4.1 Electrochemical impedance spectroscopy 6

4.2 Linear sweep voltammetry 8

4.3 Tafel analysis 8

4.4 Cyclic voltammetry (activation) curves 9

4.5 Overpotential summary 10

4.6 Long-term stability (chronopotentiometry) 10

4.7 Post-synthesis morphology (SEM) 12

5 Discussion **13**

6 Limitations and Future Work **14**

7 Conclusion **15**

References **15**

1 Introduction

Water electrolysis is limited on the anodic side by the oxygen evolution reaction (OER), a sluggish four-electron/four-proton process with a high thermodynamic potential (1.23 V vs RHE) and slow O–O bond formation kinetics. Replacing OER with the oxidation of a small, more easily dehydrogenated molecule is an established strategy for cutting the overall cell voltage needed for electrolytic hydrogen production. Urea oxidation (UOR) is a particularly attractive substitute: it has a much lower theoretical potential (~0.37 V vs RHE) than OER, and coupling it to hydrogen production simultaneously treats urea-containing wastewater, turning a pollutant into an energy-saving co-reactant.

Ni- and Co-based materials are the leading non-precious-metal candidates for both OER and UOR in alkaline media, since their surface hydroxide/oxyhydroxide phases are the true catalytically active species. Zeolitic imidazolate frameworks (ZIFs) are an appealing precursor route to such materials: their regular, N-rich, high-surface-area structure can be converted directly into metal/metal-oxide nanostructures embedded in (or supported on) N-doped carbon by controlled pyrolysis, without needing a separate carbon source.

This project benchmarks three electrodes, all grown on the same Ni foam (NF) substrate and tested under identical conditions: (i) bare Ni foam as the control, (ii) ZIF-67-derived Co/CoNC@NF (Co-based), and (iii) ZIF-8-derived NC@NF (Zn-based). Because Zn is volatile at the pyrolysis temperature used here (1050 °C, well above Zn's boiling point of 907 °C) while Co is not, ZIF-8 pyrolysis is expected to leave behind an N-doped carbon coating with little to no residual active metal, making it a partial “blank” control against which the genuinely metal-containing ZIF-67-derived catalyst can be judged. This gives the comparison a built-in internal logic: Ni foam (metallic, unmodified) vs. ZIF-8/NC@NF (carbon-only) vs. ZIF-67/Co-CoNC@NF (metal + carbon).

Two points about the present dataset are stated up front, in the interest of transparency, and are revisited in Section 6: (1) all electrochemical results below are expressed as geometric current density, since the catalyst-coated working-electrode area is fixed at 1 cm^2 for every sample (Section 3.2); however, the electrochemically active surface area (ECSA) of each electrode was not independently measured, so these values should not yet be read as ECSA-normalized intrinsic activity; and (2) LSV curves were recorded without on-instrument iR compensation, so Tafel slopes were corrected post hoc using each sample's own EIS-derived solution resistance rather than a real-time compensated measurement.

2 Related Work

Because ZIF-derived Co/Ni electrocatalysts are most extensively documented in the adjacent field of electrocatalytic nitrate reduction to ammonia (eNO3RR), the related-work context here is drawn primarily from that literature; the underlying catalyst-design logic — engineering the metal/N-doped-carbon interface to tune electronic structure and active-site accessibility — is directly transferable to OER/UOR.

- Wu et al. (Nat. Commun. 2025) show that residual lattice oxygen and lattice tensile strain in oxide-derived Cu nanosheets jointly tune intermediate adsorption and *H supply, lowering the energy barrier for a multi-electron electrocatalytic reaction — the same lattice-strain/electronic-modulation logic used here to rationalize why Co-based ZIF-67 outperforms Zn-based ZIF-8.
- Zou et al. (Angew. Chem. Int. Ed. 2024) demonstrate a MOF-on-MOF Ni-BDC@Co-HHTP heterostructure in which interfacial Ni–O–Co bonds create two distinct, complementary active sites (Ni for substrate adsorption, Co for hydrogenation) — directly analogous to the metal/N-doped-carbon dual environment expected in our Co/CoNC@NF electrode.
- Zhang et al. (Nat. Commun. 2023, Fe/Cu diatomic catalyst) and Liu et al. (Angew. Chem. Int. Ed. 2022, Rh@Cu) both show that pairing a substrate-activating metal with a hydrogen-supplying co-catalyst on a shared support outperforms either single-metal system alone, supporting the general principle that the carbon/heteroatom environment surrounding a metal center is not a passive scaffold but an active participant in catalysis.
- Han et al. (Nat. Catal. 2023) and Liu et al. (Angew. Chem. Int. Ed. 2026, alkali-metal cation effects) both illustrate that electrocatalytic performance for multi-step, multi-electron reactions is frequently governed by a trade-off between two competing sub-steps (there: substrate adsorption vs. active-hydrogen supply) rather than by either alone — the same framing we use in Section 5 to interpret the Tafel-slope and pre-wave differences between Ni, ZIF-8, and ZIF-67.
- Directly on the materials side, Liu et al. (J. Colloid Interface Sci. 2023) synthesized Co nanoparticle-decorated N-doped carbon by pyrolyzing ZIF-67 and used it as a standalone electrocatalyst, reporting that the Co/N-doped-carbon interface enhances electron transfer — direct precedent for treating our ZIF-67-derived Co/CoNC@NF as an active catalyst rather than a mere support.
- Separately, ZIF-8-derived N-doped carbon is repeatedly used in the wider literature specifically as a metal-free control or catalyst support (e.g., for the oxygen reduction reaction), because Zn is lost during high-temperature pyrolysis — supporting our treatment of ZIF-8/NC@NF as a partial “blank” baseline rather than a third independently active catalyst.

Gap addressed: none of the above works directly compares ZIF-8- and ZIF-67-derived electrodes against a common Ni-foam control across both OER and UOR under matched synthesis and electrochemical protocols. This project provides that side-by-side benchmark, using a shared activation, LSV, Tafel, and EIS protocol across all three electrodes and both electrolytes.

3 Methodology

3.1 Materials synthesis

ZIF-67@NF: 0.6 g cobalt(II) nitrate hexahydrate was dissolved in 10 mL methanol; separately, 0.6 g 2-methylimidazole was dissolved in 10 mL methanol. A piece of Ni foam (~1 cm × 3 cm), pre-treated in 3 M HCl, was immersed in the 2-methylimidazole solution, and the cobalt nitrate solution was then added dropwise with stirring. The mixture was stirred for 4 h to allow in situ growth of ZIF-67 on the Ni foam surface, then washed and dried under vacuum at 60 °C. The dried sample was pyrolyzed in a tube furnace under Ar at 1050 °C for 2 h to give the final Co/CoNC@NF electrode.

ZIF-8@NF: the same procedure was followed, substituting zinc nitrate hexahydrate for cobalt nitrate hexahydrate, to give ZIF-8@NF and, after the same 1050 °C pyrolysis step, NC@NF.

3.2 Electrochemical measurements

All measurements used a conventional three-electrode cell on a Gamry Interface 1010E workstation at room temperature: the catalyst-coated Ni foam (1 cm × 1 cm) as working electrode, Ag/AgCl (saturated KCl) as reference, and a graphite rod as counter electrode. This gives a fixed geometric working-electrode area of exactly 1 cm^2; consequently, every current value reported in Sections 4–5 is expressed as geometric current density (mA cm^{-2}), numerically equal to the raw measured current. Measured potentials were converted to the RHE scale via:

$$\mathbf{E\ (vs.\ RHE) = E\ (vs.\ Ag/AgCl) + 0.197 + 0.0597 \times pH}$$

which for 1 M KOH (pH ≈ 14) gives a fixed conversion offset of 1.0328 V; this offset was verified to be numerically exact and consistent across every recorded LSV/CV dataset.

- Activation: 50 cycles of CV at 50 mV s^{-1} from 1.1 to 1.6 V (vs RHE), allowing the working-electrode surface to electrochemically reconstruct.
- Performance evaluation: LSV at 5 mV s^{-1} (forward scan) in 1 M KOH and 1 M KOH + urea.
- Surface re-equilibration: 3 further CV cycles after LSV, prior to EIS.
- EIS: potentiostatic, recorded at the potential corresponding to 10 mA cm^{-2}, 5 mV AC amplitude, 0.01 Hz–100 kHz.

3.3 Data analysis

LSV and CV data were processed in OriginPro; EIS spectra were fit in ZView using an Rs(CPE–Rp) equivalent circuit (solution resistance in series with a constant-phase-element/charge-transfer-resistance parallel combination). This circuit was selected because every spectrum showed a single depressed semicircle with no obvious diffusion tail, indicating charge-transfer-controlled behaviour rather than mass-transport control. Because raw Tafel slopes drifted substantially with the choice of fitting window — a signature of uncompensated ohmic resistance compounded by evolving surface state and reaction kinetics during the sweep — each LSV was additionally iR-corrected in Python using the Rs value from that same sample's own EIS fit (E_corrected = E_RHE − I × Rs) before Tafel slopes were extracted. Onset potentials and overpotentials at fixed currents (10 mA cm^{-2} and 50 mA cm^{-2}, geometric current density, since the working-electrode area is 1 cm^2; see Section 6 for the remaining ECSA caveat) were extracted from the RHE-converted, non-iR-corrected LSV curves for direct comparability with the as-measured data.

4 Results

4.1 Electrochemical impedance spectroscopy

Nyquist spectra (Figure 1) were fit sample-by-sample; Rs was well-constrained in every case (<2.5% error) and was used for the iR correction in Section 4.3. Rp (charge-transfer resistance) was only loosely

constrained for several samples, most severely ZIF-67 + urea, where the Nyquist arc does not close within the measured frequency window.

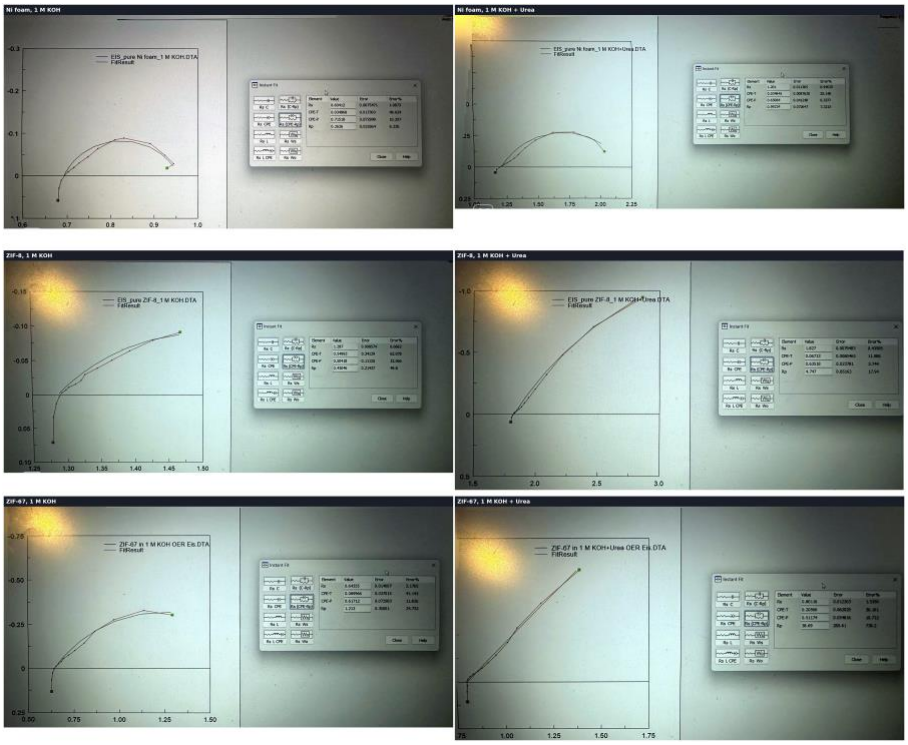


Figure 1. Nyquist plots (points) with ZView fit overlay (line) and Instant-Fit parameter tables, all six sample/electrolyte combinations.

Sample	Rs (Ω)	Rs err %	Rp (Ω)	Rp err %	Fit quality
Ni foam, KOH	0.694	1.1%	0.263	8.3%	Usable
Ni foam, KOH+Urea	1.201	0.9%	0.992	7.3%	Good
ZIF-8, KOH	1.287	0.7%	0.430	49.8%	Rp unreliable
ZIF-8, KOH+Urea	1.827	0.4%	4.747	17.9%	Marginal
ZIF-67, KOH	0.644	2.2%	1.213	24.7%	Marginal
ZIF-67, KOH+Urea	0.801	1.5%	38.69	738%	Rs usable; Rp unresolved

4.2 Linear sweep voltammetry

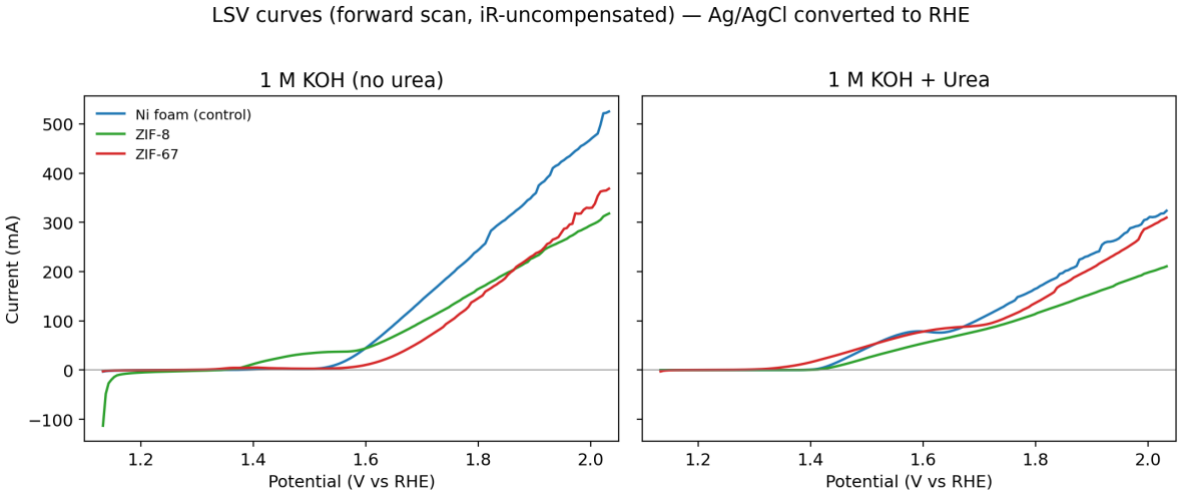


Figure 2. LSV curves (forward scan), control (Ni foam) vs. ZIF-8 vs. ZIF-67, pure KOH (left) vs. KOH + urea (right).

Ni foam and ZIF-67 (pure KOH) both show a pre-OER hump/shoulder around 1.3–1.5 V vs RHE, corresponding to the electrochemical oxidation of Ni^{2+}/Ni^{3+} (or Co^{2+}/Co^{3+}) prior to oxygen evolution, i.e. an $M(OH)_2$ → MOOH surface redox transition rather than catalytic OER onset; ZIF-8 does not show this feature. With urea added, all three electrodes show a distinct low-potential wave that plateaus — most plausibly mass-transport-limited urea oxidation, though surface reaction kinetics cannot be excluded as a contributing cause — before true OER current resumes at higher potential; this feature is clearest for Ni and ZIF-67 and weak/absent for ZIF-8.

4.3 Tafel analysis

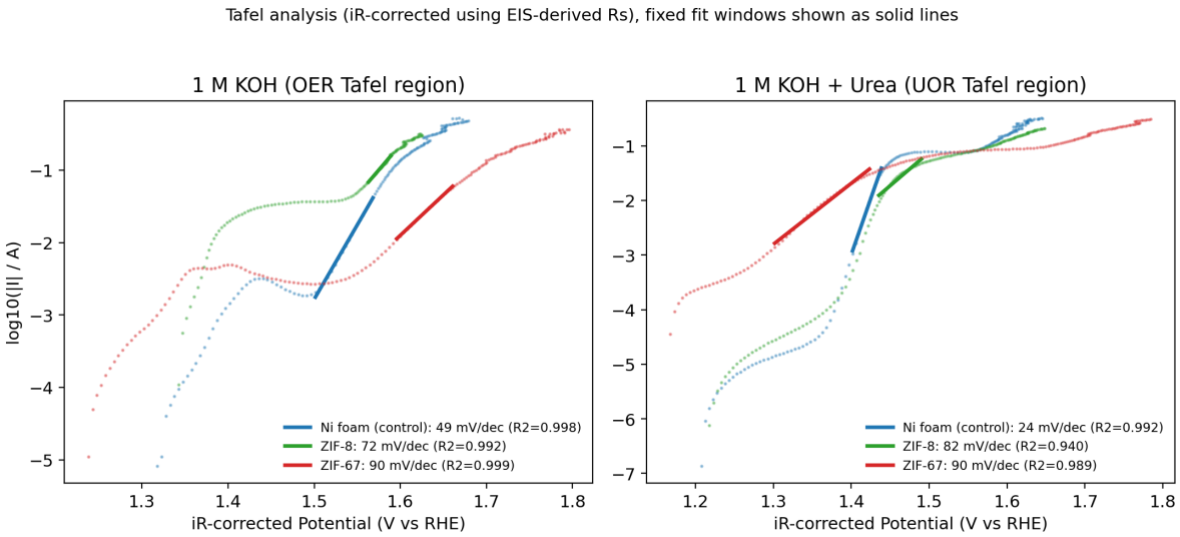


Figure 3. Tafel plots (iR-corrected), OER region (pure KOH, left) and UOR region (KOH + urea, right).

Sample	Fit window (V vs RHE)	Slope (mV/dec)	R^2

Ni foam, KOH (OER)	1.50 – 1.60	49	0.998
ZIF-8, KOH (OER)	1.65 – 1.80	72	0.992
ZIF-67, KOH (OER)	1.60 – 1.70	90	0.999
Ni foam, KOH+Urea (UOR)	1.40 – 1.48	24	0.992
ZIF-8, KOH+Urea (UOR)	1.45 – 1.58	82	0.940
ZIF-67, KOH+Urea (UOR)	1.30 – 1.45	90	0.989

4.4 Cyclic voltammetry (activation) curves

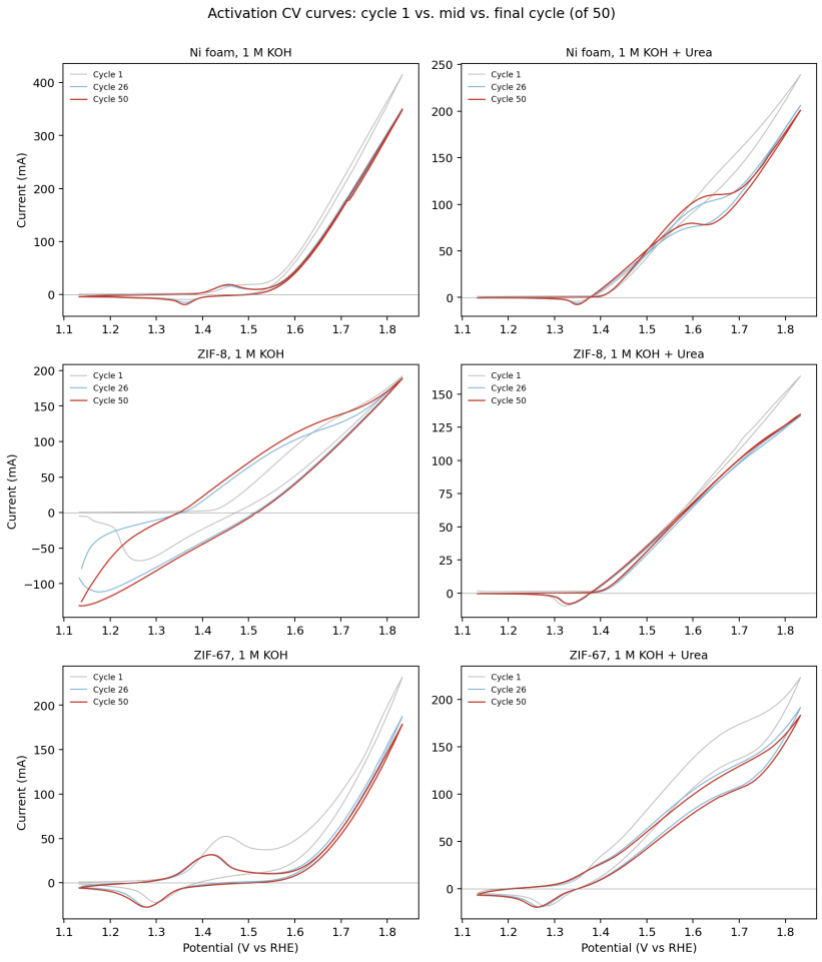


Figure 4. Activation CV evolution (cycle 1 vs. mid-cycle vs. final cycle of 50), all six sample/electrolyte combinations.

All six samples show the expected activation behaviour: current density in the OER/UOR region increases from cycle 1 toward the final cycle, consistent with progressive surface reconstruction and the formation of catalytically active oxyhydroxide species, then largely stabilizes by the later cycles —

indicating that the 50-cycle activation protocol had converged for all samples before LSV data were collected.

4.5 Overpotential summary

Onset potential (first zero-current crossing) and overpotential (η = E_RHE − 1.23 V, OER reference) or oxidation potential at fixed geometric currents of 10 mA cm^{-2} and 50 mA cm^{-2}, read directly from the RHE-converted LSV curves.

Sample	Onset (V vs RHE)	η/E @ 10 mA cm^{-2} (mV)	η/E @ 50 mA cm^{-2} (mV)
Ni foam, KOH	1.315	316	376
ZIF-8, KOH	1.340*	164	385
ZIF-67, KOH	1.235†	369	456
Ni foam, KOH+Urea	1.205	205	279
ZIF-8, KOH+Urea	1.215	224	354
ZIF-67, KOH+Urea	1.165†	146	275

** ZIF-8 (pure KOH) shows a large initial capacitive transient (−113 mA decaying to ~0 by 1.32 V) that likely biases this zero-crossing; its low apparent η@10 mA cm^{-2} should therefore be read with caution rather than taken at face value as superior intrinsic activity.*

† Ni foam and ZIF-67 (pure KOH) onset is picked up by the $M(OH)_2$/MOOH pre-wave, not true catalytic OER onset — their η@10 mA cm^{-2} / η@50 mA cm^{-2} values are the more reliable activity comparison.

4.6 Long-term stability (chronopotentiometry)

To assess operational durability under UOR conditions, the ZIF-67-derived Co/CoNC@NF electrode was subjected to a galvanostatic (constant-current) chronopotentiometric hold at 100 mA cm^{-2} in 1 M KOH + urea for approximately 26 h, with the potential (vs. Ag/AgCl) recorded at 1 s intervals (Figure 5). The point-to-point potential drift rate, |dE/dt|, was computed from the raw time series and plotted on a logarithmic scale against time (Figure 6) to evaluate how quickly the electrode approached a quasi-steady operating state.

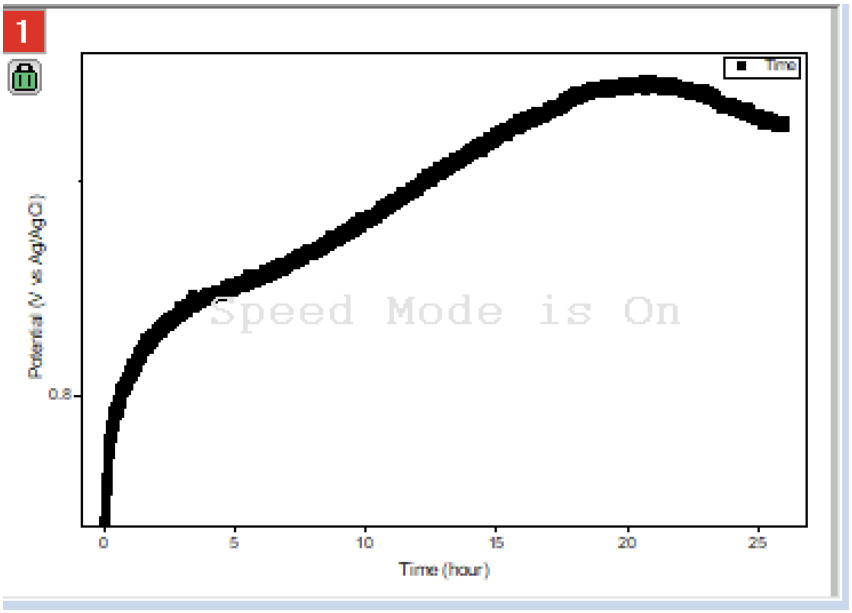


Figure 5. Chronopotentiometric hold at 100 mA cm^{-2} (constant current), ZIF-67/Co-CoNC@NF in 1 M KOH + urea, ~26 h.

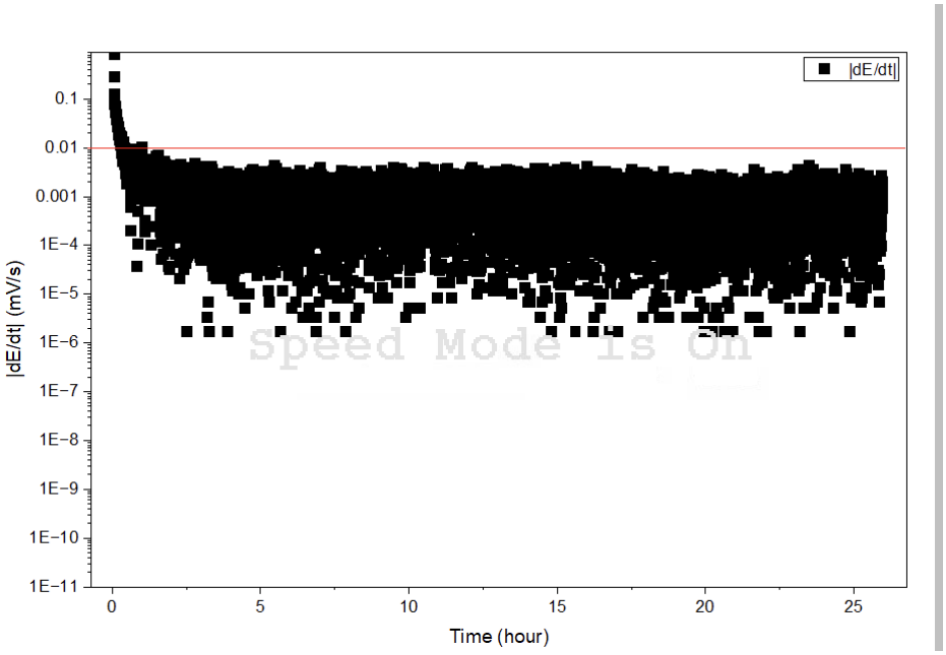


Figure 6. Potential drift rate |dE/dt| (log scale) vs. time for the same run, with a reference line at |dE/dt| = 0.01 mV/s marking the approximate onset of quasi-steady-state operation.

The potential rises steeply over the first ~2 h as the electrode surface reconstructs under load, then increases more gradually until reaching a broad maximum around 19–21 h, before declining slightly toward the end of the test. This non-monotonic potential evolution may arise from several factors, including continued surface reconstruction, changes in active surface area, reactant depletion, or mass-transport effects; additional post-test characterization is required to distinguish these contributions, rather than catastrophic failure. Consistent with this, the drift-rate analysis shows |dE/dt| falling below the 0.01 mV/s reference line within approximately the first 1–1.5 h of the hold and remaining below it

for the great majority of the remaining ~24–25 h, punctuated only by sparse, brief excursions. This indicates the electrode reaches a quasi-steady operating potential rapidly and sustains it over an extended period at a practically relevant current density (100 mA cm^{-2}). This stability test was performed for the ZIF-67/Co-CoNC@NF electrode under UOR conditions only; Ni foam, ZIF-8, and pure-KOH (OER) stability remain to be tested (Section 6).

4.7 Post-synthesis morphology (SEM)

Scanning electron microscopy (SEM, 15.0 kV, secondary-electron imaging) was used to examine the surface morphology of the two ZIF-derived coatings on Ni foam after pyrolysis. Both electrodes retain the underlying open-cell Ni foam scaffold (struts of order 100 µm; Figures 7a and 8a,b), confirming the coating process does not collapse the foam's macroporous architecture.

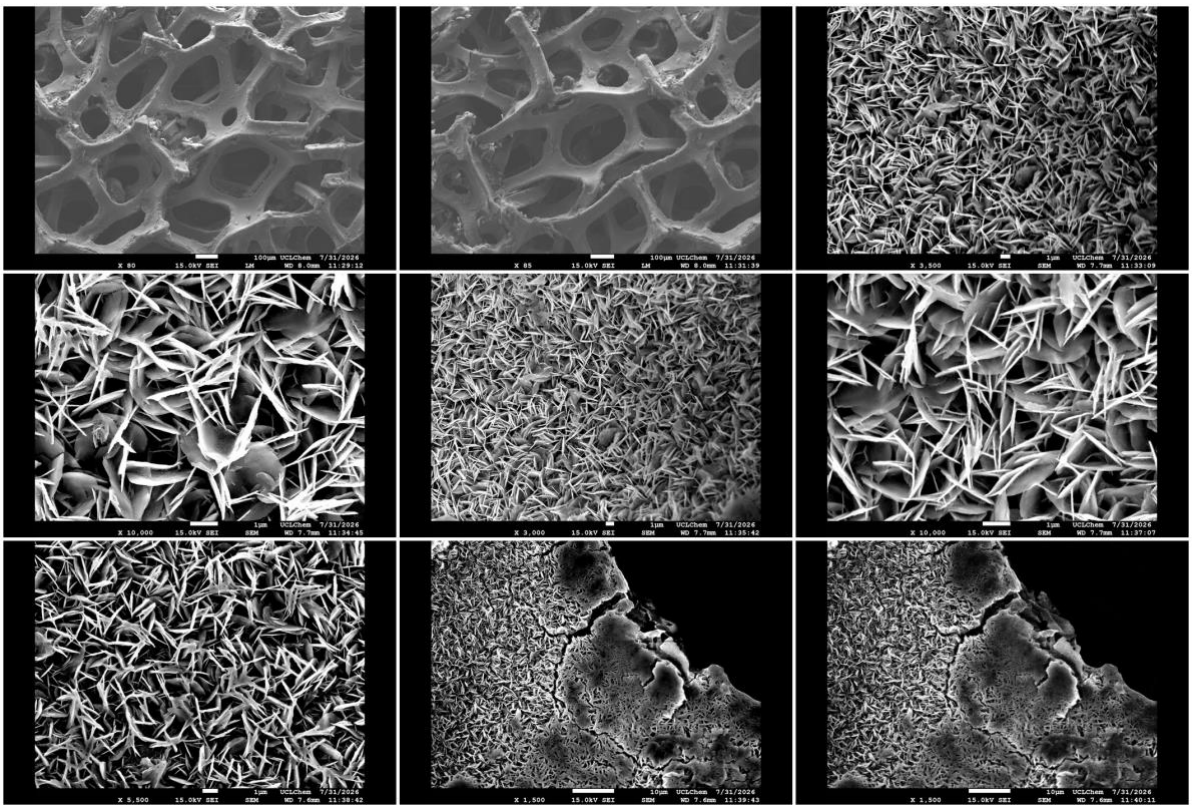


Figure 7. SEM images of the ZIF-8-derived NC@NF electrode at increasing magnification (X80 to X13,000), showing the Ni foam scaffold uniformly coated with a dense mat of thin, blade/needle-like nanostructures.

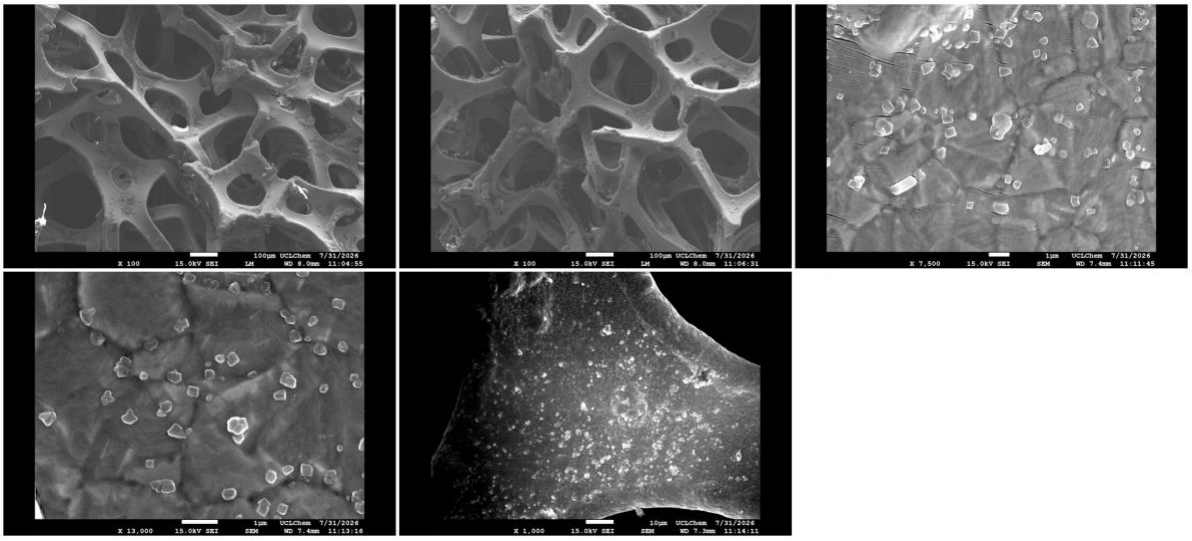


Figure 8. SEM images of the ZIF-67-derived Co/CoNC@NF electrode at increasing magnification (X100 to X13,000), showing a smoother, cracked ("mudflat"-textured) coating on the Ni foam struts with sparse, discrete faceted micro-crystallites.

The two coatings are morphologically distinct. ZIF-8/NC@NF (Figure 7) displays a dense, uniform layer of thin, blade/needle-like nanostructures covering essentially the entire strut surface, with this texture consistent from X1,500 through X10,000. ZIF-67/Co-CoNC@NF (Figure 8), by contrast, shows a comparatively smooth, cracked surface texture at low-to-medium magnification, with only sparse, small, faceted (cubic/polygonal) particles visible at higher magnification (X7,500–X13,000), rather than a continuous needle-like layer. This confirms that the two pyrolyzed coatings are structurally distinct, consistent with the different precursor chemistries described in Section 1; however, attributing either morphology specifically to metal retention or loss would require the compositional (XPS/EDS) confirmation noted in Section 6, and is not claimed on the basis of SEM imaging alone.

5 Discussion

The headline numbers in Section 4.5 tell two different stories depending on electrolyte. In pure KOH, ZIF-8 shows the lowest apparent η@10 mA cm^{-2} (164 mV), but this is the sample most affected by an initial capacitive transient and by not showing the $M(OH)_2$/MOOH pre-wave at all — i.e. its apparent "early" activity is not accompanied by the same redox chemistry seen in Ni and ZIF-67, and should not be read as ZIF-8 being the most catalytically active OER electrode. Judged instead by Tafel-slope quality and consistency, ZIF-67 is the most well-behaved catalyst in pure KOH (R^2 = 0.999, essentially window-insensitive after iR correction), consistent with genuine Co-based catalytic character rather than a capacitive artifact.

The urea results are more straightforward to interpret and meet expectations: adding urea lowers the oxidation potential for all three electrodes relative to pure KOH, and ZIF-67 becomes clearly the best performer (146 mV at 10 mA cm^{-2}, lowest of the three), consistent with Co being an intrinsically strong urea-oxidation catalyst in alkaline media. The UOR Tafel slopes (24, 82, 90 mV dec^{-1} for Ni, ZIF-8, ZIF-67) diverge substantially between electrodes — an unexpected finding, since all three were subjected to the

same activation protocol and electrolyte. Ni foam's markedly lower Tafel slope (24 mV dec^{-1}) suggests a different rate-determining step on the reconstructed Ni-oxyhydroxide surface compared with the carbon-supported ZIF-derived electrodes, and is worth targeted follow-up (Section 6).

This is further supported by post-synthesis SEM imaging (Section 4.7): ZIF-8-derived electrodes display a dense, uniform layer of thin blade/needle-like nanostructures, whereas ZIF-67-derived electrodes show a smoother, cracked surface with only sparse faceted micro-crystallites, confirming the two coatings are structurally distinct — though, as noted in Section 4.7, linking this morphology directly to metal retention requires the XPS/EDS confirmation listed in Section 6.

The supplementary stability test (Section 4.6) adds a further, independent line of evidence in ZIF-67's favour: at a practically relevant current density (100 mA cm^{-2}), the electrode reaches a quasi-steady operating potential within 1–1.5 h and sustains it for the great majority of a ~26 h hold, indicating the reconstructed active surface is not merely active but reasonably durable under sustained UOR operation — though this was only tested for one electrode and one condition (Section 6).

Overall, across both OER and UOR conditions, ZIF-67 (Co-based) is the strongest-performing catalyst by onset potential, Tafel-slope quality, and demonstrated short-term stability; Ni foam is a solid, reliable control; and ZIF-8 (Zn-based) is consistently the weakest of the three once the capacitive-artifact caveat is accounted for — a coherent, chemically sensible result set, although further validation using ECSA-normalized current densities and improved EIS fitting is required before this can be established as a definitive activity ranking.

6 Limitations and Future Work

- All results in this report are normalized to the geometric area of the catalyst-coated Ni foam working electrode (1 cm × 1 cm = 1 cm^2; Section 3.2), so current values are reported throughout as geometric current density (mA cm^{-2}). However, the electrochemically active surface area (ECSA) — which can differ substantially from the geometric area, especially for the porous, ZIF-derived coatings — was not independently measured (e.g., via double-layer capacitance). Next step: measure ECSA (via Cdl) for each electrode and re-express results as ECSA-normalized current density for a fairer comparison of intrinsic activity.
- The ZIF-67 + urea EIS fit is not usable quantitatively (738% error on Rp) because the Nyquist arc does not close within the measured frequency window. Next step: re-measure EIS at this condition with a lower minimum frequency, or re-fit with additional physically motivated constraints.
- Tafel slopes remain somewhat fitting-window-dependent for Ni and ZIF-8 even after iR correction. Next step: agree on and document one fixed fitting-window convention (e.g. a defined current-density range) to apply uniformly across all six sample/electrolyte combinations.
- The RHE conversion constant (1.0328 V) should be reconfirmed against the exact Ag/AgCl fill-solution type and a directly measured electrolyte pH, rather than the nominal pH 14 assumed for 1 M KOH.
- No product analysis (e.g. quantification of N_2, CO_2, or other UOR products) was performed, so Faradaic efficiency for urea oxidation is currently unknown. Next step: couple chronoamperometry with a suitable product-quantification method (colourimetric, GC, or NMR) to determine UOR

selectivity, following the isotope-labelling / colourimetric approaches used broadly in the adjacent nitrate-reduction literature reviewed in Section 2.

- A single long-term chronopotentiometric stability test (100 mA cm^{-2}, ~26 h) has now been run for the ZIF-67/Co-CoNC@NF electrode under UOR conditions (Section 4.6), showing the potential drift rate falling below 0.01 mV/s within ~1–1.5 h and remaining there for most of the run. However, Ni foam and ZIF-8 have not yet been tested for stability, nor has any electrode been tested under pure-KOH (OER) conditions. Next step: repeat the stability protocol across all three electrodes and both electrolytes, paired with post-test SEM/XRD to check whether the reconstructed active phase is retained.
- Composition of the two ZIF-derived electrodes has not been directly confirmed by XPS or EDS; the assumption that ZIF-8 largely loses its Zn during 1050 °C pyrolysis (leaving mainly N-doped carbon) is inferred from literature precedent and the SEM morphology in Section 4.7 rather than measured directly on these samples. Next step: acquire XPS/EDS on both electrodes, pre- and post-activation, to confirm elemental composition and any surface reconstruction.

7 Conclusion

This project benchmarked Ni foam, ZIF-8-derived NC@NF, and ZIF-67-derived Co/CoNC@NF for OER and UOR in alkaline media using a matched activation, LSV, Tafel, and EIS protocol. In pure KOH, Ni foam and ZIF-67 both show a $Ni/Co(OH)_2 \rightarrow MOOH$ pre-wave and comparable Tafel quality, while ZIF-8's lower apparent onset is most likely a capacitive artifact rather than genuine superior activity. With urea added, the picture sharpens: ZIF-67 requires only 146 mV to reach 10 mA cm^{-2} — the lowest of the three electrodes — consistent with cobalt's well-established intrinsic activity for urea oxidation, while Tafel slopes (24, 82, and 90 mV dec^{-1} for Ni, ZIF-8, and ZIF-67) reveal that the three electrodes operate under distinctly different reaction kinetics despite identical synthesis and testing conditions. A preliminary chronopotentiometric test further shows that the ZIF-67/Co-CoNC@NF electrode reaches a quasi-steady operating potential within ~1–1.5 h and sustains it over ~26 h at 100 mA cm^{-2}, a promising early indicator of operational durability that should be extended to the other two electrodes and to OER conditions. Post-synthesis SEM confirms the ZIF-8- and ZIF-67-derived coatings are morphologically distinct, though linking this to metal retention specifically awaits compositional confirmation. Taken together, the results support ZIF-67-derived Co/CoNC@NF as the most promising of the three electrodes for combined OER/UOR catalysis, while underlining that a definitive activity ranking still requires ECSA-normalized current densities and a fully resolved EIS fit for the ZIF-67 + urea condition. The main takeaway: the identity of the metal center embedded in a ZIF-derived, N-doped-carbon-on-Ni-foam architecture — not the ZIF framework itself — is the dominant factor controlling alkaline OER/UOR performance in this system.

References

[1] Q. Wu, X. Fan, B. Shan, L. Qi, X. Quan, Y. Liu, “Insights into lattice oxygen and strains of oxide-derived copper for ammonia electrosynthesis from nitrate,” Nat. Commun. 16, 3479 (2025).

[2] S. Zhang, J. Wu, M. Zheng, X. Jin, Z. Shen, et al., “Fe/Cu diatomic catalysts for electrochemical nitrate reduction to ammonia,” Nat. Commun. 14, 3634 (2023).

[3] Y. Zuo, M. Sun, T. Li, L. Sun, S. Han, Y. Chai, B. Huang, X. Wang, “Capturing copper single atom in proton donor stimulated O-end nitrate reduction,” Adv. Mater. 37, 2415632 (2025).

[4] X. Liu, B. Mao, Y. Shen, X. Ma, F. Du, D. Wang, L. Zhao, X. Chen, C. Hu, “Steering intermediate coupling by alkali-metal cations for efficient nitrate electroreduction to ammonia,” Angew. Chem. Int. Ed. e3670039 (2026).

[5] Y. Zou, Y. Yan, Q. Xue, C. Zhang, T. Bao, et al., “MOF-on-MOF heterostructured electrocatalysts for efficient nitrate reduction to ammonia,” Angew. Chem. Int. Ed. 63, e202409799 (2024).

[6] H. Liu, X. Lang, C. Zhu, J. Timoshenko, M. Rüscher, et al., “Efficient electrochemical nitrate reduction to ammonia with copper-supported rhodium cluster and single-atom catalysts,” Angew. Chem. Int. Ed. 61, e202202556 (2022).

[7] S. Han, H. Li, T. Li, F. Chen, R. Yang, Y. Yu, B. Zhang, “Ultralow overpotential nitrate reduction to ammonia via a three-step relay mechanism,” Nat. Catal. 6, 402–414 (2023).

[8] P. H. van Langevelde, I. Katsounaros, M. T. M. Koper, “Electrocatalytic nitrate reduction for sustainable ammonia production,” Joule 5, 290–294 (2021).

[9] H. Liu, J. Qin, J. Mu, B. Liu, “In situ interface engineered Co/NC derived from ZIF-67 as an efficient electrocatalyst for nitrate reduction to ammonia,” J. Colloid Interface Sci. 636, 134–140 (2023).